Hemostatic bioactivity and mechanism of novel *Rubia cordifolia* L.-derived carbon dots

Zhaojiong Zhang, Wenjing Hu, Aiqi Yu, Haixue Kuang and Meng Wang [ID] *

Background: *Rubia cordifolia* L. (RCL) Carbonisata is a typical calcined natural medicinal plant, which has been used for thousands of years for hemostasis. At present, some studies have shown that some components of processed RCL Carbonisata can enhance hemostasis, but the specific hemostatic material basis is still unclear. Novel carbon dots (CDs) were obtained from *Rubia cordifolia* L. and named RCL-CDs to explore the hemostatic effect and mechanism of RCL-CDs obtained from *Rubia cordifolia* L. *Methods*: RCL-CDs were characterized by transmission electron microscopy (TEM), high-resolution transmission electron microscopy (HRTEM), Fourier transform infrared spectroscopy (FT-IR), ultraviolet visible spectroscopy (UV-Vis), fluorescence spectroscopy (FL), X-ray diffraction (XRD), and X-ray photoelectron spectroscopy (XPS). The hemostatic effect of RCL-CDs was evaluated in a mouse tail amputation model and liver scratch model, and the hemostatic mechanism was explored using a capillary coagulation model and coagulation parameters. *Results*: The particle size distribution of RCL-CDs ranged from 1.74 nm to 9.78 nm, the maximum population was 3–4 nm, and the average particle size was 3.82 nm. The RCL-CDs were approximately spherical with a lattice spacing of 0.206 nm. The quantum yield (QY) of RCL-CDs is 1.09%, and there is a distinct diffraction peak at $2\theta = 24.76°$. The elemental composition of RCL-CDs was mainly C (65.28%), O (30.10%), and a small amount of N (4.62%). Pharmacological experiments showed that bleeding time and bleeding volume were reduced in mice treated with RCL-CDs. It is worth noting that the low-, medium- and high-dose RCL-CD groups can significantly reduce the blood loss, while the high-dose RCL-CD group can significantly reduce the bleeding time of the mouse tail amputation model and liver scratch model. Additionally, the fibrinogen level (FIB) and platelet counts (PLT) increased and prothrombin time (PT) decreased in rats after treatment with RCL-CDs. *Conclusions*: RCL-CDs have a significant hemostatic effect, and the mechanism may be exogenous coagulation and activation of fibrinogen. This explains the material basis of the hemostatic effect of RCLC and opens new avenues for more in-depth investigation. In addition, new insights into the potential biomedical applications of CDs in the field of nanohemostasis are provided and a solid foundation for the discovery of novel hemostatic agents is established.

Introduction

Human history is essentially a record of the struggle against disease. Epidemics or infectious diseases have appeared alongside the progress of human civilization, exerting profound and comprehensive impacts on it. They are often more severe than war, revolution and insurrection, because they directly hit the core of civilization and the most fundamental of all productive factors—human beings themselves, affecting their bodies and hearts. Hemorrhagic diseases have accompanied mankind throughout history. Hemorrhagic diseases, defined as diseases caused by abnormal hemostasis mechanisms, are a major global public health problem.[1] Uncontrolled bleeding is one of the leading causes of death in humans, which occurs mainly before reaching the emergency department due to excessive blood loss, and rapid and effective hemostasis after bleeding can reduce bleeding and mortality.[2,3] At present, hemostasis for tissue surface bleeding caused by external forces is mainly achieved by physical compression, surgical suturing, medical dressings, or drug therapy.[4-6] Physical compression can quickly stop bleeding, but prolonged compression can lead to local ischemia and even tissue necrosis. Surgical suturing promotes tissue regeneration and healing by aligning the edges of the wound, but it can also lead to issues such as wound necrosis. Medical dressings such as collagen sponges and growth factor gels provide an environment conducive to cell growth, while stimulating angiogenesis and promoting granulation tissue and epithelial cell regeneration, but they also have high costs and immunogenicity issues. The most commonly used antibiotics in drug therapy can also cause gastrointestinal

Key Laboratory of Basic and Application Research of Beiyao, Ministry of Education, Heilongjiang University of Chinese Medicine, Harbin, 150000, China. E-mail: wangmeng06TCM@163.com

discomfort, allergic reactions, and even drug resistance.[7,8] Therefore, it is important to develop hemostatic materials with high biological safety.

The theory of treating bleeding with charcoal is first found in Ge Kejiu's Book of Ten Medicines, which has a history of more than 2000 years.[9] The application of charcoal frying with traditional Chinese medicine to hemostasis is a major feature of Chinese medicine and plays an important role in the use of traditional Chinese medicine (TCM) in past dynasties. *Rubia cordifolia* L. (RCL) is a perennial herbaceous climbing plant in the Rubiaceae family, which is widely distributed in India, Korea, Africa, tropical Asia, Malaysia, Europe and China, and the root or rhizome of RCL in China is called Qiancaogen or Chien-tsao.[10,11] In India, RCL is known as Madder or India Madder and is locally known as "Manjistha". Moreover, RCL has been used in Ayurveda for the treatment of various inflammations and to promote wound healing.[12] Not only in India, RCL is used in many parts of the world. RCL is a traditional medicine used in Korea to treat dysmenorrhea, arthritis, bleeding and urinary diseases.[13] RCL is used in Unani medicine to treat various skin diseases, in the Philippines to treat urinary tract infections and in Uganda to treat tuberculosis. In traditional Asian medicine, RCL has become an important drug for the treatment of many types of bleeding.[14] Modern studies show that RCL mainly contains alizarin, purpurin, *etc.*, which have obvious effects on promoting blood coagulation.[15,16] As a hemostatic agent, RCL has been listed in the Chinese Pharmacopoeia. *Rubia cordifolia* L. Carbonisata (RCLC) is the product of high temperature carbonization of RCL, which has been widely used in clinical treatment of endogenous and exogenous hemorrhage. Clinical studies have shown that the RCLC increases 1,3-dihydroxy-2-ethoxymethyl-9,10-anthraquinone and enhances the hemostatic effect, but the hemostatic material basis and mechanism of RCLC are still unclear.[17] For years, efforts have been made to elucidate the pharmacological basis of carbon-based medicines' hemostatic action from the perspective of micromolecular activators, but these efforts have been unsuccessful, prompting us to turn our attention to new substances generated after the carbonization of drugs, namely carbon dots (CDs).

CDs are a new type of zero-dimensional carbon nanomaterial with a diameter of less than 10 nm and have good biocompatibility, low cytotoxicity, stable fluorescence characteristics and comprehensive functionality.[18-20] Due to the significant advantages of CDs, the improvement of related applications provides many strategies for finding modern drugs that can successfully control or treat some diseases. CDs have attracted significant attention from medical researchers in biosensing, bioimaging, nanomedicine, and drug delivery.[21,22] It is important to note that CDs extracted from charcoal drugs are considered to be obtained from natural products, which is in line with the bottom-up preparation of CDs. At present, CDs obtained from charcoal drugs have been proved to have different physical and chemical properties and biological activities. For example, SCR-CDs obtained from scrambled *Coptidis Rhizoma* can treat ulcerative colitis in mice, and SRC-CDs obtained from *Scutellariae Radix* carbonisata have antiallergic effects.[23,24] PRAC-CDs obtained from *Paeoniae Radix* Alba carbonisata have a hepatoprotective effect and CPO-CDs obtained from carbonized *Platycladus orientalis* have a hemostatic effect.[25] It is noteworthy that hemostatic effects represent the main research direction of charcoal drugs. CDs derived from charcoal drugs retain certain pharmacological properties of the original TCM and may impart broader medical value through their unique nanostructures. Furthermore, these plant-derived CDs are non-toxic and readily accessible, addressing the challenges of multiple side effects and high costs associated with current hemostatic methods. This suggests that they may serve as a foundational material for novel hemostatic agents and pave the way for innovative directions in drug research.

On this basis, we discovered and identified new CDs from high temperature processed charred RCL, which were not found in the original herb, named them RCL-CDs, and characterized them. We subsequently evaluated their hemostatic effect and the mechanism of hemostasis.

Experimental

Plant materials and chemicals

RCL, harvested in Sichuan province, was purchased from Harbin Yutai Pharmaceutical Co., Ltd (Heilongjiang, China). Hemocoagulase (HC) for injection was purchased from Jinzhou Ahon Pharmaceutical Co., Ltd (Liaoning, China). Experimental chemical reagents (analytical grade) were obtained from Tianjin Fuyu Fine Chemical Co., Ltd (Tianjin, China). Dialysis bags with a 1.0 kDa molecular weight cut-off were purchased from Beijing Biotopped Technology Co., Ltd (Beijing, China). The water used in the experiment was deionized water (DW).

Animals

All experimental procedures were in accordance with the Regulations for the Administration of Affairs Concerning Experimental Animals approved by the State Council of the People's Republic of China. The animal experimental design and protocols used in this study were approved by the Ethics Review Committee for Animal Experimentation at the Heilongjiang University of Chinese Medicine. 80 Specific Pathogen Free (SPF) grade Kunming male rats (weighing 20.0 ± 2.0 g) and 40 Sprague–Dawley (SD) rats (weighing 200.0 ± 20.0 g) were purchased from Liaoning Changsheng Bio-technology Co., Ltd (Liaoning, China). The animals were placed in a well-ventilated room with a temperature of 24.0 ± 1.0 °C, a relative humidity of 55–65%, and a light/dark cycle of 12 h. The animals are allowed to eat and drink at will, but they were fasted for 12 h before the experiment.

Preparation of RCL-CDs

100 g of RCL was weighed and placed in a crucible, sealed with aluminum foil, covered with a lid, and placed in a muffle furnace (YTH-2.5-10; Shaoxing Supo Instrument Co., Ltd, Zhejiang, China). In Phase I, the temperature of the muffle furnace was increased up to 70 °C within 5 min and maintained there for 30 min. In Phase II, it was increased up to 350 °C within

25 min and maintained there for 1 h. After the RCLC is naturally cooled, the crude product is ground into powder using a multifunctional crusher (800C; Yongkang Red SUN Electromechanical Co., Ltd, Zhejiang, China). The powder was passed through a 60-mesh sieve and then dissolved in DW with 15 times the mass of carbon powder and soaked for 30 min, and boiled three times in a water bath at 100 °C, and each treatment lasted for 1 h. The resulting black solution was collected, coarse filtered, and then fine filtered through a 0.22 μm cellulose membrane (Shanghai Xingya Purification Material Factory, Shanghai, China). The solution was concentrated to approximately 40 mL using a rotary evaporator (N-1300; Tokyo Riken Instrument Co., Ltd, Japan), and then dialysis was performed for 72 hours using a 1.0 kDa dialysis membrane, and the dialysate was changed at 3 h intervals. Finally, the aqueous extract containing RCL-CDs was stored at 4 °C for further experiments. The preparation process for RCL-CDs is shown in Fig. 1.

Characterization of RCL-CDs

Transmission electron microscopy (TEM; Tecnai G2 F30; FEI Company, USA) was utilized to recognize and characterize RCL-CDs. The water extract of RCL-CDs was sonicated for 0.5 h, passed through a 0.22 μm filter membrane, aspirated with a 1 mL syringe, and added dropwise to the center of the copper mesh. Natural air drying or assisted drying ensures that the sample is completely dry before TEM observation. TEM magnifying lens working at 100 kV and high-resolution TEM (HRTEM; JEN-1230; Japan Electron Optics Laboratory; Japan) pictures at 200 kV were utilized to see the morphology and estimate dispersion of RCL-CDs. The spectral properties of the RCL-CDs were examined utilizing ultraviolet-visible (UV-Vis; UV-3600; Jindao Company, Japan) and fluorescence spectroscopy (FL; S1000/FS5; Edinburgh Company, UK). Meanwhile, Fourier transform infrared (FT-IR; 8400S; Shimadzu Company, Japan) was used to identify the organic functional groups within the spectral range of 400–4000 cm^{-1}. X-ray photoelectron spectra (XPS; ESCALAB 250XI; Thermo Scientific Company, USA) were recorded to identify the elements and the organic functional groups. X-ray diffraction (XRD; Bruker D8 Advance; Bruker Company, Germany) was performed with Cu K-α radiation. The RCL-CDs used for XRD testing should be powdered to ensure that the particle size of the powder is less than 70 μm (over 200 mesh). The scanning voltage was set to 40 kV, the current to 40 mA, and the scanning range to 10°–90°.

Quantum yield of RCL-CDs

The fluorescence quantum yield (QY) of RCL-CDs was determined using quinine sulfate as a standard (% QY = 54 in 0.1 M H_2SO_4 solution), with the calculation formula as follows:[26,27]

$$Q_{CDs} = Q_R \times \frac{I_{CDs}}{I_R} \times \frac{A_R}{A_{CDs}} \times \frac{\eta_{CDs}{}^2}{\eta_R{}^2}$$

In the formula, Q represents QY, I represents the integral area under the emission spectrum, A represents the absorbance wavelength, and η represents the solvent refractive index. Subscripts 'CDs' and 'R' refer to RCL-CDs and the standard, respectively. In order to minimize the reabsorption effect and ensure the accuracy of the results, both A_R and A_{CDs} were maintained below 0.05.

Hemostatic effect of RCL-CDs

The experimental models of tail amputation and liver injury in mice were established according to previous studies, and appropriate modifications were made.[28,29] Briefly, 80 SPF grade Kunming male rats (weighing 20.0 ± 2.0 g, 40 of each model) were randomly assigned to one of the five experimental groups (n = 8 per group): the control group received normal saline (NS, A1); the HC group received 0.1 KU mL^{-1} HC solution (B1); and the low-(C1), medium-(D1) and high-(E1) dose RCL-CD groups received 0.078 g mL^{-1}, 0.156 g mL^{-1}, abs 0.312 g mL^{-1} RCL-CD solutions, respectively. HC injection was given subcutaneously, and the other drugs were given by gavage, with a dose of 0.2 mL. After 1 h of administration, anesthesia was induced in all animals by intraperitoneal injection of 0.3% (0.2 mL 30 g^{-1}) sodium pentobarbital.

In the tail amputation model, using aseptic surgical scissors, the mouse tails were cut at a point approximately 0.82–0.93 mm in diameter (about 10 mm from the tip). Immediately after, each tail was placed on a piece of filter paper.

In the liver scratch model, the midline of the mouse abdomen was cut with clean surgical scissors to expose the liver, a procedure that must ensure that the mice survive, and the livers of the mice were padded with saline infiltrated gauze. The left lateral lobe of the liver was scratched with a 5 mL syringe, causing liver bleeding, so as to determine the liver injury, and then the incision was covered with filter paper.

The bleeding is monitored every 30 s until it stops.[30] The end point of hemostasis is defined as maintaining hemostasis for 30 min, while recording the stopping time of hemostasis and

Fig. 1 Flow diagram of the preparation process of *Rubia cordifolia* L.-carbon dots (RCL-CDs).

the amount of bleeding. All mice were sacrificed by cervical dislocation at the end of the experiment.

Note that the grouping and administration personnel were not consistent with the observers of subsequent experiments, and the groups indicated by the observers is only indicated as groups A1, B1, C1, D1, and E1. This ensured that the experiment used a blind experimental method to avoid subjective factors that could interfere with the experimental results.

Hemostatic mechanism of RCL-CDs

The hemostatic mechanism was determined using a capillary coagulation model and coagulation parameter measurement. 40 Sprague–Dawley (SD) rats weighing 200.0 ± 20.0 g were randomly divided into 5 groups ($n = 8$ per group): control (NS, A2); HC (B2, 0.1 KU mL^{-1}); and low- (C2), medium- (D2), and high- (E2) dose RCL-CDs (0.078, 0.156 and 0.312 g mL^{-1}, respectively). HC injection was given subcutaneously, and the other drugs were given by gavage, with a dose of 0.2 mL.

In the capillary coagulation model, the posterior orbital venous plexus of the mice was punctured with a capillary glass tube, and the blood was allowed to flow naturally, wiping off the first drop of blood. A second drop of blood was aspirated with a capillary glass tube until the lumen was filled. A small section of capillary glass tube about 5–10 mm is broken every 30 s, until there is blood connection between the two sections of the glass tube. Maintaining hemostasis for 30 min was defined as the end point of hemostasis, and the stopping time of hemostasis and the amount of blood loss were recorded.

After 1 h of subcutaneous injection, blood samples were obtained from the abdominal aorta of rats and placed in a plastic tube containing 3.2% sodium citrate (citrate/blood: 1/9, v/v). They were left at room temperature (24 ± 1 °C) for at least 1 h. Then, the samples were centrifuged at 3500 rpm in a centrifuge (KL05A; Kaida Scientific Instrument Co., Ltd, Hunan, China) for 10 min to obtain plasma. And then, an automatic coagulation analyzer (C2000-A; Puli Sheng Instrument Co., Ltd, Beijing, China) was used to measure prothrombin time (PT), activated partial thromboplastin time (APTT), thrombin time (TT), and fibrinogen levels (FIB). Platelet counts (PLT) were measured using an automatic five-category blood analyzer (XS-500i; Sysmex Corporation, Japan).[31]

Note that the grouping and administration personnel were not consistent with the observers of subsequent experiments, and the groups indicated by the observers is only indicated as groups A2, B2, C2, D2, and E2. This ensured that the experiment used a blind experimental method to avoid subjective factors that could interfere with the experimental results.

Statistical analysis

SPSS (version 25.0, Chicago, IL) was used for statistical analysis. The data of non-normal distribution are represented by medians, while the data of normal distribution and homogeneous variance are represented by mean standard deviations. One-way analysis of variance (ANOVA) was used for multiple comparisons, and then the least significant (LSD) difference test was conducted. $P < 0.05$ indicated statistically significant
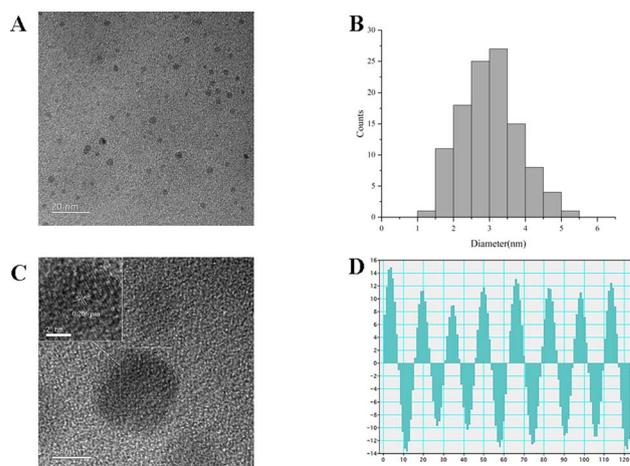

Fig. 2 Characterization of RCL-CDs. (A) Transmission electron microscopy (TEM) images of *Rubia cordifolia* L.-carbon dots (RCL-CDs) displaying ultra-small particles. (B) Histogram depicting particle size distribution. (C) High-resolution TEM (HRTEM) image of RCL-CDs. (D) The inset shows a HRTEM image of atomic lattice fringes.

differences, and $P < 0.01$ indicated statistically extremely significant differences.

Results

Characterization of RCL-CDs

In this study, RCL-CDs extracted from RCL were characterized. As shown in Fig. 2A, the TEM image of RCL-CDs clearly shows that CDs were spherical and monodisperse, with the size distribution between 1.74 and 9.78 nm, and the largest population is located at 3–4 nm. The average size in Fig. 2B is 3.82 nm. In addition, HRTEM shows that the lattice spacing of CDs is 0.206 nm (Fig. 2C) and HRTEM images are shown in Fig. 2D.
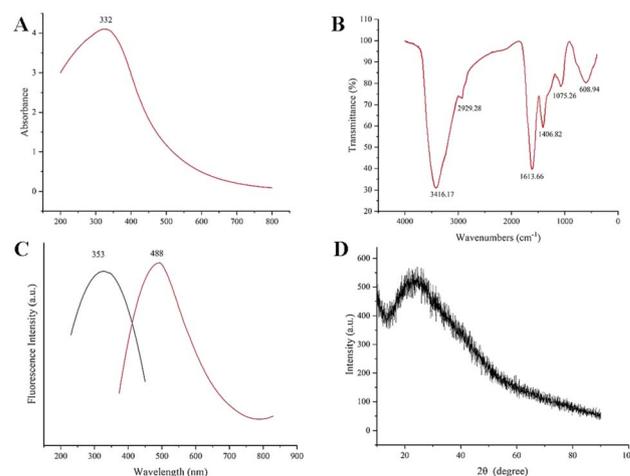

Fig. 3 The ultraviolet-visible, Fourier transform infrared, fluorescence spectroscopy and X-ray diffractometer spectrum of analyses of RCL-CDs. (A) The UV-vis spectrum of RCL-CDs. (B) The FT-IR spectrum of RCL-CDs. (C) The FL spectrum of RCL-CDs. (D) The XRD spectrum of RCL-CDs.

The optical properties of RCL-CDs were determined by UV-vis spectrum analysis. The UV-Vis spectrum (Fig. 3A) of an aqueous solution of RCL-CDs shows a weak absorption peak at 332 nm, which can be attributed to the $\pi-\pi*$ transition of aromatic C=C bonds. Furthermore, the FL spectra showed the maximum emission at 488 nm and the maximum excitation at 353 nm, as displayed in Fig. 3C. Taking quinine sulfate as a reference, the QY of RCL-CDs was calculated to be 1.09%. Moreover, as can be seen from Fig. 3D, there is an obvious diffraction peak ($2\theta = 24.76°$) in the XRD spectrum, which is caused by the disordered arrangement of amorphous carbon atoms.

To better understand the organic functional groups on the surface of the RCL-CDs, we further analyzed the CDs using FT-IR spectroscopy, and the spectra of the purified RCL-CDs (Fig. 3B) show characteristic peaks at 3416, 2929, 1613, 1406, 1075 and 608 cm^{-1}. The peak at 3416 cm^{-1} indicates the presence of the O–H groups. The peak at 2929 cm^{-1} is attributed to the C–H groups, which may be due to the presence of methylene groups associated with aliphatic hydrocarbons in RCL-CDs. The presence of an absorption peak at 1613 cm^{-1} indicates the presence of C=C groups. The peak at 1406 cm^{-1} is the bending vibration of saturated C–H, possibly from methyl or methylene groups. In addition, C–C or C–O groups are present at 1075 cm^{-1}. Simultaneously, the peak of RCL-CDs at 608 cm^{-1} is the result of the existence of C–C groups.[32,33]

Fig. 4 The surface composition and elemental analysis of the prepared RCL-CDs by XPS. (A) X-ray photoelectron spectroscopy spectra of the RCL-CDs; high resolution (B) C1s, (C) O1s and (D) N1s peaks of the RCL-CDs.

The surface composition and elemental analysis of the prepared RCL-CDs were characterized using an XPS technique. As shown in Fig. 4A, peaks were evident at 295.18 eV, 400.28 eV, and 541.28 eV, indicating that the quantum dots are mainly composed of C, O and N, accounting for 65.28%, 30.10% and 4.62%, respectively. The C1s spectrum (Fig. 4B) was deconvoluted into four peaks at 284.80, 285.83, 286.64 and 288.39 eV, corresponding to C–C, C–N, C–O, and C=O carboxyl groups. The O1s spectrum (Fig. 4C) was divided into two peaks at 531.42 and 532.91 eV, attributed to C–O and C=O, respectively. Furthermore, Fig. 4D shows the N1s spectrum with peaks at 400.37 and 399.22 eV, corresponding to different chemical environments for C–N and H–N. In addition, Ca and Mg elements have also been found in RCL-CDs.

Hemostatic effect of RCL-CDs

The mouse tail amputation model and liver scratch model were used to investigate the hemostatic effect of RCL-CDs, and the results were that both models showed that RCL-CDs reduced bleeding time and blood loss.

In the mouse tail amputation model, in terms of bleeding time, compared to the NS group (12.88 ± 0.74 min), the bleeding time of the HC group and high-dose RCL-CD group (5.13 ± 0.64 and 8.25 ± 0.96 min, respectively) significantly decreased ($P < 0.01$), and the bleeding time of the middle- and low-dose RCL-CD treatment groups (11.69 ± 0.53, 11.94 ± 0.62 min, respectively) slightly decreased ($P < 0.05$). In terms of blood loss, the blood loss of the HC group, and high-, middle- and low-dose RCL-CD groups was 0.0551 ± 0.006, 0.1439 ± 0.0113, 0.1698 ± 0.0091 and 0.2055 ± 0.0128 g, respectively (Table 1). Compared with the NS group (0.3171 ± 0.0112 g), they were significantly decreased ($P < 0.01$), as shown in Fig. 5.

In the liver scratch model, from bleeding time, the bleeding time in the HC group (4.50 ± 0.65 min) significantly decreased ($P < 0.01$) compared with the NS group (9.31 ± 0.59 min), the bleeding time in the high-dose RCL-CD treatment group (5.88 ± 0.74 min) slightly decreased ($P < 0.05$), and the bleeding time in the middle- and low-dose RCL-CD groups (8.44 ± 0.90 and 8.88 ± 0.74 min, respectively) had no significant difference (Table 2). From blood loss, HC group, high-, middle- and low-doses of RCL-CD groups, the bleeding (0.1347 ± 0.0128, 0.2466 ± 0.0226, 0.4339 ± 0.5517, and 0.0187 ± 0.0132 g, respectively) significantly decreased ($P < 0.01$), compared with the NS group (0.6496 ± 0.0198 g), as shown in Fig. 6.

Hemostatic mechanism of RCL-CDs

To determine the hemostatic mechanism of the RCL-CDs, we established a capillary coagulation model and measured the clotting parameters PT, APTT, TT, FIB, and PLT in SD rats.
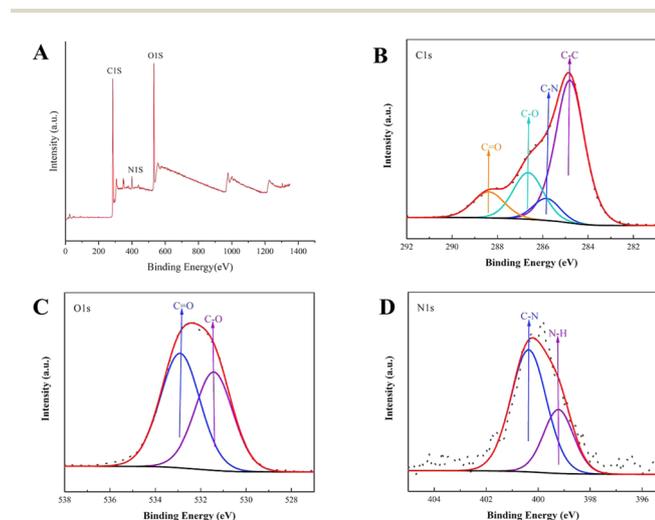
Table 1 Bleeding time and blood loss in the tail amputation model

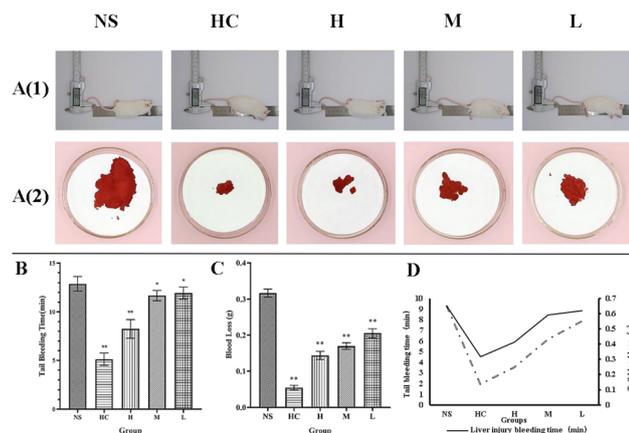| Groups	Dose	Tail bleeding time (min)	Tail blood loss (g)
NS	—	12.88 ± 0.74	0.3171 ± 0.0112
HC	0.100 KU mL^{-1}	$5.13 \pm 0.64**$	$0.0551 \pm 0.0060**$
High-dose RCL-CDs	0.312 g mL^{-1}	$8.25 \pm 0.96**$	$0.1439 \pm 0.0113**$
Middle-dose RCL-CDs	0.156 g mL^{-1}	$11.69 \pm 0.53*$	$0.1698 \pm 0.0091**$
Low-dose RCL-CDs	0.078 g mL^{-1}	$11.94 \pm 0.62*$	$0.2055 \pm 0.0128**$

Fig. 5 Mouse model of the severed tail. (A) (1) The appearance of the mouse tail diameter. (2) Apparent amount of bleeding after tail amputation in the mouse. (B)–(D) The mice were treated with NS (control), HC, or the indicated concentrations of RCL-CDs ($n = 8$ per group). *$P < 0.05$; **$P < 0.01$, as compared with the control group.
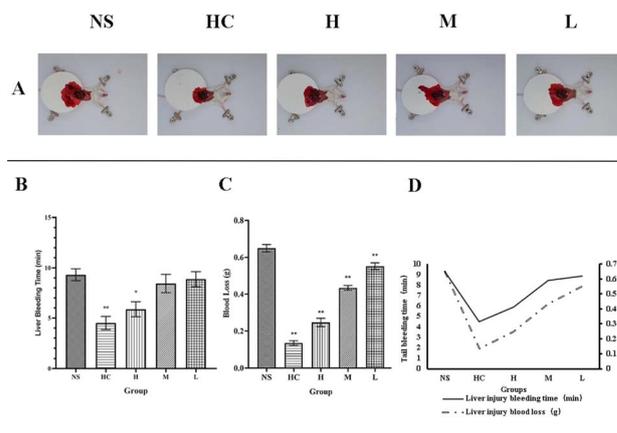

Fig. 6 Liver scratch model. (A) Presentation of bleeding from liver injury. (B)–(D) The mice were treated with NS (control), HC, or the indicated concentrations of RCL-CDs ($n = 8$ per group). *$p < 0.05$; **$p < 0.01$, as compared with the control group.

In the capillary coagulation model, compared with the NS group (165.00 ± 27.77 s), the blood coagulation time of the HC group (60.00 ± 22.68 s) significantly decreased ($P < 0.01$) and the blood coagulation time of the high- and middle-dose RCL-CD treatment groups (108.75 ± 31.82, 127.50 ± 31.05 s, respectively) significantly decreased ($P < 0.01$) (Table 3). No significant difference was found in bleeding time between the NS group (165.00 ± 27.77 s) and low-dose RCL-CD group (138.75 ± 31.82 s), as shown in Fig. 7.

The low-dose RCL-CD group did not show any significant differences in PT, APTT, or TT compared to the NS group. And there were no significant differences in the APTT and TT of RCL-CDs between the high- and middle-dose groups (Table 4). PT values of the HC group and high-dose RCL-CD treatment group (12.02 ± 0.34 and 12.96 ± 0.19 s, respectively) significantly decreased ($P < 0.01$), and the PT of the middle-dose RCL-CD treatment group (13.53 ± 0.29 s) significantly decreased ($P < 0.05$). And the APTT and TT values of the HC group (19.43 ± 0.31 and 42.78 ± 0.82 s, respectively) have a significant difference ($P < 0.05$). In addition, significant increases ($P < 0.01$) in the FIB and PLT were observed in HC, high-, middle- and low-dose RCL-CD treatment groups (60.00 ± 22.68 [1527.13 ± 34.22], 2.29 ± 0.18 [1442.88 ± 36.86], 2.23 ± 0.10 [1366.63 ± 38.46] and 2.22 ± 0.11 [1329.00 ± 30.53] g mL^{-1} (10^9 L^{-1}), respectively). The results are presented in Fig. 8.

Table 3 Clotting time in the capillary coagulation model

Groups	Dose	Capillary clotting time (s)
NS		165.00 ± 27.77
HC	0.100 KU mL^{-1}	60.00 ± 22.68**
High-dose RCL-CDs	0.312 g mL^{-1}	108.75 ± 31.82*
Middle-dose RCL-CDs	0.156 g mL^{-1}	127.50 ± 31.05*
Low-dose RCL-CDs	0.078 g mL^{-1}	138.75 ± 31.82

Discussion

As a traditional charcoal drug, RCLC has been used for thousands of years to stop bleeding. Hemostasis is a very complex self-repair process, and it is also an important step in medical and emergency medicine. The process involves promoting vascular contraction, activating the coagulation system, inhibiting the fibrinolytic system effect, and promoting platelet aggregation.[34–36] At present, the research on the hemostatic mechanism of carbon drugs primarily focuses on coagulation and anticoagulation systems, the fibrinolysis system and platelet reactions.[37] Although studies have attempted to elucidate the components of its hemostatic effect from a phytochemical point of view, it remains unclear. The process of carbon medicine processing is a process of "high temperature carbonization", which is very similar to the preparation of modern nanomaterials, "CDs" (spherical nanoparticles with

Table 2 Bleeding time and blood loss in the liver injury model

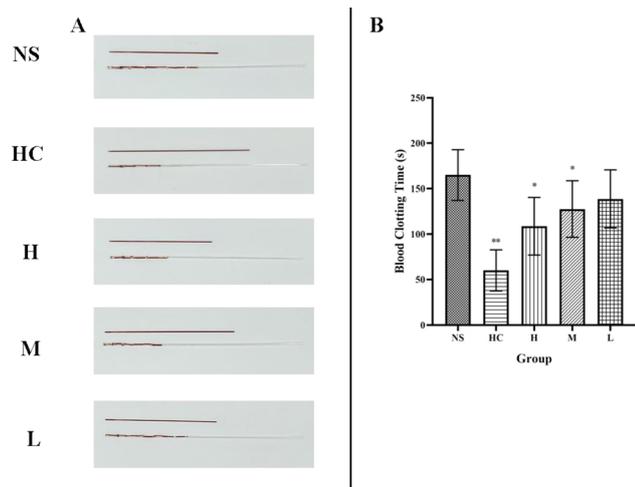| Groups	Dose	Liver injury bleeding time (min)	Liver injury blood loss (g)
NS		9.31 ± 0.59	0.6496 ± 0.0198
HC	0.100 KU mL^{-1}	4.50 ± 0.65**	0.1347 ± 0.0128**
High-dose RCL-CDs	0.312 g mL^{-1}	5.88 ± 0.74*	0.2466 ± 0.0226**
Middle-dose RCL-CDs	0.156 g mL^{-1}	8.44 ± 0.90	0.4339 ± 0.0132**
Low-dose RCL-CDs	0.078 g mL^{-1}	8.88 ± 0.74	0.5517 ± 0.0187**

Fig. 7 Capillary blood coagulation model. (A) Visual demonstration of capillary coagulation. (B) The mice were treated with NS (control), HC, or the indicated concentrations of RCL-CDs ($n = 8$/group). *$p < 0.05$; **$p < 0.01$, as compared with the control group.

Fig. 8 Graphs of measurements of coagulation parameters. (A) Prothrombin time (PT); (B) activated partial thromboplastin time (APTT); (C) thrombin time (TT); (D) fibrinogen (FIB); (E) platelets (PLT); (F) overall comparison of coagulation parameters. There were five groups ($n = 8$ per group): normal control group (NS), HC group (1.0 KU mL^{-1}) and groups with different concentrations of RCL-CDs group. *$p < 0.05$; **$p < 0.01$, compared with the control group.

particle sizes less than 10 nm and a carbon skeleton structure). We changed the way of thinking, considering the technology and methods introduced into the TCM carbon nanoresearch in the study of medicine.

In this study, new CDs were found and extracted from RCL, and they were identified as RCL-CDs and characterized by TEM, HRTEM, FT-IR, UV-Vis, FL, XRD and XPS. The average particle size of RCL-CDs was 3.82 nm and the lattice spacing was 0.206 nm, which was observed by TEM and HRTEM. The elemental composition and structure of RCL-CDs were determined by XRD, FT-IR and XPS. RCL-CDs is mainly composed of carbon with a graphite structure, the constituent elements are C, N and O, and contains C=N, C=O, C–OH and other functional groups. The FL spectrum showed that 332 nm was the maximum excitation wavelength of RCL-CDs, and 353 nm was the maximum emission wavelength.

In the present study, we evaluated the hemostatic effect of RCL-CDs using mouse tail amputation and liver scratch models, and the results showed that the prepared RCL-CDs effectively controlled bleeding, shortened bleeding time, and reduced bleeding volume compared with the control group in both models. To investigate the mechanism of hemostasis, we constructed a capillary coagulation model and measured coagulation parameters. The results showed that the clotting time of HC and RCL-CDs was shorter than that of the control group,
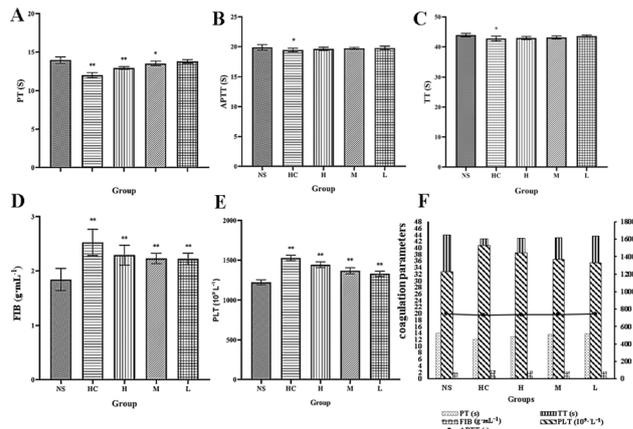
and the FIB and PLT contents of RCL-CDs increased, PT decreased, and APTT and TT did not change significantly compared with the control group. In general, the coagulation pathway includes both the endogenous and exogenous pathways.[38] Clinical expressed in APTT endogenous clotting pathway, and PT is used for clinical evaluation index extrinsic coagulation pathway.[39] TT and FIB are commonly used indicators of the common pathway of coagulation and are associated with promoting the conversion of FIB from soluble fibrinogen to insoluble fibrin.[40] The effect of RCL-CDs on FIB and PT, but not APTT, indicates that the coagulation pathway of RCL-CDs is related to the exogenous coagulation system and the activated fibrinogen system. The core of this hemostatic mechanism lies in RCL-CDs, which maybe utilize the unique charge properties of their surface to initiate a series of complex coagulation cascade reactions.[41] This process accelerates the activation process of platelets and cleverly combines with the external coagulation pathway to achieve the hemostatic effects. In addition, the large number of carboxyl structural units contained in RCL-CDs further strengthens the interaction forces between them and various blood cells, providing additional assistance and stability for the coagulation process.[42] This study is a preliminary investigation into the hemostatic effects and mechanisms of RCL-CDs, and further research is needed to clarify the underlying mechanism. In addition, the discovery of

Table 4 Various coagulation parameters in different groups

Groups	Dose	PT (s)	APTT (s)	TT (s)	FIB (g mL^{-1})	PLT (10^9 L^{-1})
NS		13.96 ± 0.40	19.88 ± 0.47	43.95 ± 0.56	1.84 ± 0.20	1224.00 ± 31.97
HC	0.100 KU mL^{-1}	12.02 ± 0.34**	19.43 ± 0.31*	42.78 ± 0.82*	2.53 ± 0.24**	1527.13 ± 34.22**
High-dose RCL-CDs	0.312 g mL^{-1}	12.96 ± 0.19**	19.62 ± 0.28	42.97 ± 0.51	2.29 ± 0.18**	1442.88 ± 36.86**
Middle-dose RCL-CDs	0.156 g mL^{-1}	13.53 ± 0.29*	19.72 ± 0.16	43.15 ± 0.53	2.23 ± 0.10**	1366.63 ± 38.46**
Low-dose RCL-CDs	0.078 g mL^{-1}	13.79 ± 0.22	19.77 ± 0.31	43.60 ± 0.34	2.22 ± 0.11**	1329.00 ± 30.53**

RCL-CDs in RCLC and their enhanced hemostatic effect provided a theoretical basis for the study of RCLC and other charcoal drugs.

CDs, as an emerging nanomaterial, have broad application prospects in the fields of biological imaging, drug/dye/protein/gene delivery, cancer diagnosis, and treatment.[43,44] CDs are an important class of fluorescent carbon-based nanomaterials with potential biomedical applications due to their good chemical stability and long body circulation.[45] Studies have shown that CDs can modulate the performance of hemostatic sponges to facilitate the absorption of wound exudate, and with the increase of CD incorporation, the hemostatic and coagulation abilities of hemostatic sponges also increase, which shows the potential of CDs as hemostatic agents and wound dressings.[46] The existing nanomedicine treatment is to reduce drug toxicity and improve drug specificity through nanotechnology, while RCL-CDs, plant-derived CDs, have negligible cytotoxicity and drug effects, which makes their applications in the field of nanohemostasis feasible.[47] In particular, RCL-CDs contain a large number of hydroxyl, carboxyl and epoxy functional groups on the surface, which can be modified to develop multifunctional nanohemostatic agents. However, despite the growing interest in the interaction between nanomaterials and life sciences, there is still a lack of studies on the activities of CDs and their action mechanisms. This study about RCL-CDs fills the gap in this aspect and lays the foundation for future drug research.

To explore further, the existing hemostatic agents include four classes, including antifibrinolytic system drugs, capillary permeability reduction drugs, coagulation factor drugs, and thrombin drugs.[48] HC is the most widely used hemostatic agent in clinical settings, and it accelerates the blood coagulation process mainly by activating the fibrinogen system, which is similar to the hemostatic mechanism of RCL-CDs.[49] However, studies have shown that HC was more effective than RCL-CDs for hemostasis, which may be related to the fact that HC can enhance capillary density and permeability, as well as its anti-inflammatory ability. Bleeding is often accompanied by inflammation, which causes the capillary walls to be damaged or permeable, allowing red blood cells to leak out of the capillaries. At the same time, it leads to leukocyte infiltration, which further destroys the structure of the vessel wall and promotes the occurrence of hemorrhage.[50] HC's ability to exert anti-inflammatory effects while stopping bleeding may be the reason for its more pronounced effect. However, HC is essentially a serine protease, which is unstable in nature and easily deteriorates, while CDs are chemically inert relative to proteases and are therefore more suitable for long-term storage. In addition, many CDs have been developed for hemostasis, such as CDs synthesized by the microwave method with glucose and urea, EYO-CDs obtained by the pyrolysis method with egg yolk oil, *etc.*[51,52] Compared with the above-mentioned CDs, RCL-CDs, as a kind of CD prepared from TCM as a carbon source, retain their pharmacological effect and also have some special functions, which are expected to exert greater medicinal value. Therefore, CDs can be used as a supplement or alternative for the treatment of bleeding in harsh environments or emergencies.

Although the hemostatic effect and mechanism of RCL-CDs have been preliminarily discussed, there are still some questions that need to be resolved. In the field of biomedical materials, the particle size of the material can affect its hemostatic effect. Specifically, small particle size can provide a large specific surface area and increase the action contact area to enhance the hemostatic effect, but such a small particle size can also lead to rapid elimination from the body, which may hinder achieving a better therapeutic effect.[53] Therefore, the particle size of RCL-CDs is the key factor affecting the hemostatic performance, and it is necessary to explore the effect of particle size on the hemostatic efficiency in order to optimize the hemostatic performance of RCL-CDs in the future. In addition, the chemical components and structures of RCL in different batches and origins may vary due to differences in the growth environment, picking time, storage conditions and other factors, which in turn affect the physicochemical properties and hemostatic effect of RCL-CDs. Future studies should perform multivariate analysis based on the origin and batch to explore how these variables specifically regulate key parameters such as the particle size distribution, surface charge, optical properties, and hemostatic effect of RCL-CDs.

Conclusions

In this study, novel CDs were obtained from RCL and characterized by TEM, HRTEM, UV-Vis, FT-IR, FL, XRD and XPS. *In vivo* pharmacodynamic experiments showed that RCL-CDs had a good hemostatic effect on the mouse tail severed model and liver scratch model. And through the determination of coagulation parameters, it was found that the hemostatic effect of RCL-CDs was realized through the exogenous coagulation system and the activation of the fibrinogen system. These results proved that the material basis of the hemostatic effect of RCLC was RCL-CDs and provided a new theoretical basis for the study of the material basis of other charcoal drugs. RCL-CDs can be used as drug delivery carriers and have hemostatic effects, showing good development potential in the field of nanohemostasis. This provides a solid foundation for the subsequent development of multifunctional CDs and provides new insights for the development of more efficient, rapid, and safe hemostatic agents by regulating the concentration of CDs to improve hemostatic performance.

Data availability

The data supporting the article have been presented in full.

Author contributions

M. W. conceptualized the project, Z. J. Z., W. J. H. and A. Q. Y. conducted the project research, Z. J. Z. and W. J. H. analysed and visualized the data, and H. X. K. provided guidance and support for the project. This manuscript was edited by Z. J. Z. All authors have agreed to the final manuscript.

Conflicts of interest

The authors declare that they have no competing interests.

Acknowledgements

Notes and references

1 P. Liang, T. Bi, Y. Zhou, C. Wang, Y. Ma, H. Xu, H. Shen, W. Ren and H. Yang, *Small*, 2023, e2303498.

2 X. Zhang, L. Jiang, X. Li, L. Zheng, R. Dang, X. Liu, X. Wang, L. Chen, Y. S. Zhang, J. Zhang and D. Yang, *Small*, 2022, **18**(3), e2101699.

3 H. He, W. Zhou, J. Gao, F. Wang, S. Wang, Y. Fang, Y. Gao, W. Chen, W. Zhang and Y. Weng, *Nat. Commun.*, 2022, **13**, 552.

4 Y. Cui, Z. Huang, L. Lei, Q. Li, J. Jiang, Q. Zeng, A. Tang, H. Yang and Y. Zhang, *Nat. Commun.*, 2021, **12**, 5922.

5 A. K. Gaharwar, P. K. Very, A. Assmann, A. Paul, G. H. McKinley, A. Khademhosseini and B. D. Olsen, *ACS Nano*, 2014, **8**, 9833–9842.

6 L. Shang, Y. Yan, Z. Li, H. Liu, S. Ge and B. Ma, *Adv. Sci.*, 2023, e2306528.

7 S. Pourshahrestani, E. Zeimaran, I. Djordjevic, N. A. Kadri and M. R. Towler, *Mater. Sci. Eng. C*, 2016, **58**, 1255–1268.

8 A. Bayır, M. Eryılmaz, M. Demirbilek, E. B. Denkbaş, I. Arzıman and M. Durusu, *Eur. J. Trauma Emerg. Surg.*, 2016, **42**(1), 77–86.

9 Z. Chen, S. Y. Ye, Y. Yang and Z. Y. Li, *Pharm. Biol.*, 2019, **57**(1), 498–506.

10 M. Wen, Q. Chen, W. Chen, J. Yang, X. Zhou, C. Zhang, A. Wu, J. Lai, J. Chen, Q. Mei, S. Yang, C. Lan, J. Wu, F. Huang and L. Wang, *Front. Pharmacol*, 2022, **13**, 965390.

11 R. B. Humbare, J. Sarkar, A. A. Kulkarni, M. G. Juwale, S. H. Deshmukh, D. Amalnerkar, M. Chaskar, M. C. Albertini, M. B. L. Rocchi, S. C. Kamble and S. Ramakrishna, *Antioxidants*, 2022, **11**(5), 1006.

12 S. Dubey and A. K. Dixit, *J. Ayurveda Integr. Med.*, 2023, **14**(2), 100688.

13 M. T. Do, Y. P. Hwang, H. G. Kim, M. Na and H. G. Jeong, *J. Cell. Physiol.*, 2013, **228**(5), 1087–1097.

14 K. Wang, L. Gao, Q. Zhang, Y. Zhang, W. Yao, M. Zhang, Y. Tang, A. Ding and L. Zhang, *J. Pharm. Biomed. Anal.*, 2020, **189**, 113475.

15 W. Zeng, Y. Fang, S. Mo, C. Shen, H. Yang, G. Luo, L. Xiao, R. Zhan and P. Yan, *Drug Des., Dev. Ther.*, 2023, **17**, 439–457.

16 L. Ford, R. L. Henderson, C. M. Rayner and R. S. Blackburn, *J. Chromatogr. A*, 2017, **1487**, 36–46.

17 A. K. Wang, T. Geng, W. Jiang, Q. Zhang, Y. Zhang, P. D. Chen, M. Q. Shan, M. Zhang, Y. P. Tang, A. W. Ding and L. Zhang, *J. Pharm. Biomed. Anal.*, 2020, **191**, 113638.

18 C. Dong, M. Xu, S. Wang, M. Ma, O. U. Akakuru, H. Ding, A. Wu, Z. Zha, X. Wang and H. Bi, *J. Nanobiotechnol.*, 2021, **19**(1), 299.

19 Y. Zhang, S. Wang, F. Lu, M. Zhang, H. Kong, J. Cheng, J. Luo, Y. Zhao and H. Qu, *J. Nanobiotechnol.*, 2021, **19**(1), 257.

20 M. Y. Pudza, Z. Z. Abidin, S. Abdul-Rashid, F. M. Yassin, A. S. M Noor and M. Abdullah, *ChemistrySelect*, 2019, **4**, 4140.

21 A. Sharma and J. Das, *J. Nanobiotechnol.*, 2019, **17**(1), 92.

22 M. Yang, H. Li, X. Liu, L. Huang, B. Zhang, K. Liu, W. Xie, J. Cui, D. Li, L. Lu, H. Sun and B. Yang, *J. Nanobiotechnol.*, 2023, **21**(1), 431.

23 Y. Mou, X. Bai, H. Ma, T. Li, Y. Zhao, T. Wu, Y. Zhang, H. Qu, H. Kong, X. Wang and Y. Zhao, *Front. Mol. Biosci.*, 2023, **10**, 1253195.

24 H. Kong, Y. Zhao, P. Cao, J. Luo, Y. Liu, H. Qu, Y. Zhang and Y. Zhao, *J. Biomed. Nanotechnol.*, 2021, **17**(12), 2485–2494.

25 Y. Z. Y. Zhang, H. K. M. Zhang, J. Cheng, J. Wu, H. Qu and Y. Zhao, *Int. J. Nanomed.*, 2020, **15**, 9049–9059.

26 C. Ding, X. Cao, C. Zhang, T. He, N. Hua and Y. Xian, *Nanoscale*, 2017, **9**(37), 14031–14038.

27 M. Y. Pudza, Z. Z. Abidin, S. Abdul-Rashid, F. M. Yassin, A. S. M Noor and M. Abdullah, *Processes*, 2019, **7**(10), 704.

28 H. Y. Zhang, K. T. Wang, Y. Zhang, Y. L. Cui and Q. Wang, *Int. J. Biol. Macromol.*, 2023, **253**(Pt 6), 127189.

29 H. Zhang, D. Pan, X. Wu, W. Su, X. Tang, D. Zhao, L. Sun, B. Song, X. Bai and X. Li, *Front. Pharmacol*, 2020, **11**, 549150.

30 Y. Zhu, Y. Qiu and L. Liao, *J. Nanosci. Nanotechnol.*, 2015, **15**(6), 4193–4199.

31 X. Yan, Y. Zhao, J. Luo, W. Xiong, X. Liu, J. Cheng, Y. Wang, M. Zhang and H. Qu, *J. Nanobiotechnol.*, 2017, **15**(1), 60.

32 Y. Wang, H. Kong, X. Liu, J. Luo, W. Xiong, Y. Zhu, Y. Zhang, Y. Zhang, Y. Zhao and H. Qu, *J. Biomed. Nanotechnol.*, 2018, **14**(9), 1635–1644.

33 X. Liu, Y. Wang, X. Yan, M. Zhang, Y. Zhang, J. Cheng, F. Lu, H. Qu, Q. Wang and Y. Zhao, *Nanomedicine*, 2018, **13**(4), 391–405.

34 Y. Ye, L. Yang, M. Leng, Q. Wang, J. Wu, W. Wan, H. Wang, L. Li, Y. Peng, S. Chai and Z. Meng, *Front. Pharmacol*, 2023, **14**, 1255069.

35 X. Wang, K. Yuan, Y. Su, X. Li, L. Meng, N. Zhao, Y. Hu, F. Duan and F. J. Xu, *Adv. Healthcare Mater.*, 2024, **13**(3), e2301945.

36 Y. Tan, Q. Yang, M. Zheng, M. T. Sarwar and H. Yang, *Adv. Healthcare Mater.*, 2024, **13**(6), e2302700.

37 S. Deng, E. Zhang, Y. Wang, Y. Zhao, Z. Yang, B. Zheng, X. Mu, X. Deng, H. Shen, H. Rong and D. Pei, *Toxicol. Lett.*, 2022, **363**, 55–66.

38 X. Yu, Z. Gao, J. Mu, H. Lian and Z. Meng, *Biomater. Sci.*, 2023, **11**(6), 2158–2166.

39 X. Zhang, Q. Yu, H. Jiang, C. Ma, H. M. David Wang, J. Wang and W. Y. Kang, *Carbohydr. Res.*, 2019, **485**, 107813.

40 C. Li, M. Hu, S. Jiang, Z. Liang, J. Wang, Z. Liu, H. D. Wang and W. Kang, *Molecules*, 2020, **25**(1), 177.

41 A. Schuck, H. E. Kim, K. M. Jung, W. Hasenkamp and Y. S. Kim, *Biosens. Bioelectron.*, 2020, **157**, 112167.

42 S. Nie, H. Qin, C. Cheng, W. F. Zhao, S. D. Sun, B. H. Su, C. S. Zhao and A. W. Gu, *J. Mater. Chem. B*, 2014, **2**(30), 4911–4921.

43 O. Bekasova, *Int. J. Biol. Macromol.*, 2024, **255**, 128181.

44 M. Abdullah, Z. Z. Abidin, S. Sobri, S. Abdul-Rashid, M. A. Mahdi, N. Azowa Ibrahim and M. Y. Pudza, *Nanomaterials*, 2019, **9**(10), 1500.

45 (*a*) M. Zeng, Y. Wang, M. Liu, Y. Wei, J. Wen, Y. Zhang, T. Chen, N. He, P. Fan and X. Dai, *Int. J. Nanomed.*, 2023, **18**, 6503–6525; (*b*) T. Ogawa, Y. Tobishima, S. Kamata, Y. Matsuda, K. Muramoto, M. Hidaka, E. Futai, T. Kuraishi, S. Yokota, M. Ohno and S. Hattori, *Front. Pharmacol*, 2021, **12**, 766406.

46 R. Shakiba-Marani and H. Ehtesabi, *Int. J. Biol. Macromol.*, 2023, **224**, 831–839.

47 R. Ahmadzadeh, S. A. Taheri, N. Mohammadi, H. Ahmed, S. V. Menon, W. R. Kadhum, A. Kumar, M. N. Shakir,

F. K. Shayan and N. Shirinkami, *J. Biochem. Mol. Toxicol.*, 2024, **38**(8), e23782.

48 R. Yegappan, J. Lauko, Z. Wang, M. F. Lavin, A. W. Kijas and A. E. Rowan, *Adv. Healthcare Mater.*, 2022, **11**(15), e2200574.

49 T. Ogawa, Y. Tobishima, S. Kamata, Y. Matsuda, K. Muramoto, M. Hidaka, E. Futai, T. Kuraishi, S. Yokota, M. Ohno and S. Hattori, *Front. Pharmacol*, 2021, **12**, 766406.

50 Y. Yao and S. E. Tsirka, *Glia*, 2012, **60**(6), 908–918.

51 D. Crista, M. Algarra, M. V. Martínez de Yuso, J. C. G. Esteves da Silva and L. Pinto da Silva, *J. Mater. Chem. B*, 2023, **11**(5), 1131–1143.

52 Y. Zhao, Y. Zhang, X. Liu, H. Kong, Y. Wang, G. Qin, P. Cao, X. Song, X. Yan, Q. Wang and H. Qu, *Sci. Rep.*, 2017, 7(1), 4452.

53 E. Fröhlich, *Curr. Med. Chem.*, 2016, **23**(5), 408–430.